MAGNETIC FIELDS FROM THE PHOTOSPHERE TO THE CORONA ASP Conference Series, Vol. 463 T. R. Rimmele, M. Collados Vera, et al., eds. © 2012 Astronomical Society of the Pacific

The Distributions of UV Solar Explosive Events

J. E. Mendoza-Torres¹ and T. Niembro-Hernandez²

Abstract. We analyze solar Explosive Events observed at the Si IV 139.37 nm emission line in raster mode with SUMER/SoHO. The spatial distributions of EE with different Doppler velocities are analyzed. Spatial offsets of the maximum of the distributions as well as the presence of two sources are commonly observed at the analyzed EE. Also, at some locations near the maximum the 0-18 km s⁻¹ distributions are similar to each other in shape and amplitude. These characteristics indicate that the red and blue Doppler EE sources could be the result of flows inside magnetic arcs.

1. Introduction

Observations in UV spectral lines formed at transition region (TR) temperatures (10^4 to 10^6 K) frequently show the so-called Explosive Events (EE) which are seen either as intensity enhancements, line profile variations or both of them (Porter & Dere 1991; Innes et al. 1997) with sizes of 2-4" and that last few minutes (see Chae et al. 1998a).

In some cases line wings enhancements reveal the presence of jets with typical Doppler shifts of $\sim 100 \ \text{km s}^{-1}$ (Chae et al. 1998b). However, it is not well known how the different velocity sources are located with respect to each other.

Many EE are first observed at spectral lines whose formation temperature corresponds to middle transition region (TR) temperatures (Mendoza-Torres et al. 2005). They are seen over the whole solar disk and are the smallest solar events observed where reconnection seems to be taking place, therefore, they could play an important role in energy transport to the Corona.

In this work observations made in June 1996 are analyzed. These are valuable data because were taken on raster observations mode that could not be further done with SUMER/SoHO after 1998. The aim is to have an insight into the behavior of plasma with different velocities at the EE sources. With this purpose we analyze the spatial distributions for different channels of the Si IV 139.37 nm line.

2. Observations

Two types of raster observations of the Si IV $\lambda 139.37$ nm line made with **a**) 40 East-West (EW) steps and **b**) 6 EW steps, are used. In both cases a 120 spatial pixels length slit, North-South oriented, where each pixel covers a 1" \times 1" field, was used.

The 40 EW positions data are obtained with time integration, per slit position, of 11.25 seconds. For 20 June a $\sim 30'' \times 120''$ region with 0'.7 EW steps is scanned

¹Instituto Nacional de Astrofísica, Óptica y Electrónica, Puebla, México

²Instituto de Geofísica, U.N.A.M Ciudad Universitaria, Coyoacan, México

Table 1. Times and locations of the observed regions, the days are all of June 1996, the EW (ini) value corresponds to the Easternmost position, EW (fin) to the Westernmost, NS (lower) to the Southermost and NS (upper) to the Northernmost locations respect the disk center.

Day	Time (UT)	Npos	EW(ini)	EW(fin)	NS(lower)	NS(upper)
20	12:07-12:31	40	-14.250	15.00	-60.0	60.0
22	16:41-17:04	40	49.625	93.69	820.125	940.120
26	02:54-03:17	40	478.625	522.69	439.875	499.875
27	12:33-12:56	40	384.562	428.62	799.125	919.120
20	13:40-14:21	6	-1.50	2.25	-60.0	60.0

(Table 1). For 22, 26 and 27 June $\sim45^{\prime\prime}\times120^{\prime\prime}$ regions are scanned with 1."1 EW steps.

In the 6 EW positions data a region of $\sim 5'' \times 120''$ is scanned with a time integration of 5 seconds at each slit position with 0.4 EW steps.

Cycles, each of two EW scans are made in each set of observations (of Table 1). In the first scan of a cycle the slit sequentially points to odd positions (for example, 1, 3, 5, ..., 39 for the 40 EW positions data) and in the second scan to the next even positions (for example, 2, 4, 6,..., 40 for the same data). For each spatial pixel a 50 pixels spectrum is obtained with a spectral resolution of 0.43 nm which corresponds to 9 km s^{-1} .

3. Data Analysis and Results

We have made routines that allow us to plot two-dimensional and one-dimensional distributions, of a given spatial region, using separately the amplitudes of various spectral channels. In Figure 1, the amplitudes for an EE, as observed at different spectral channels (each plotted on a row) are shown. The routines allow us to select the channels for which we want to build the distributions. From the most intense EE at each set of observations, five events with 40 EW positions and five with 6 EW, whose maximum took place at inner locations of the observed fields, were selected. For them, two and one-dimensional distributions were made up to 45 km s⁻¹ for the 6 EW observations and up to 130 km s⁻¹ for the 40 EW observations.

In Figure 1 the amplitudes for an EE observed with 40 EW positions are shown, the x and y axes correspond, respectively, to EW and North-South (NS) positions, an unit in the x-axis corresponds to 0.7. Blue 1 and Red 1 are for 45 km s⁻¹ and Blue 2 and Red 2 for 72 km s⁻¹. Two sources are seen at the red images, the distance between the 72 km s⁻¹ sources (bottom panels) is larger than for the 45 km s⁻¹ sources (second panels from the bottom).

In the left panel of Figure 2, the one-dimensional NS distributions across the maximum of the 45 km s⁻¹ red source of Figure 1, are shown. The radiance increase and decrease during the EE is seen. In the right panel, the one-dimensional EW distributions for the same source are shown, where the two sources are seen. From Figure 1, it

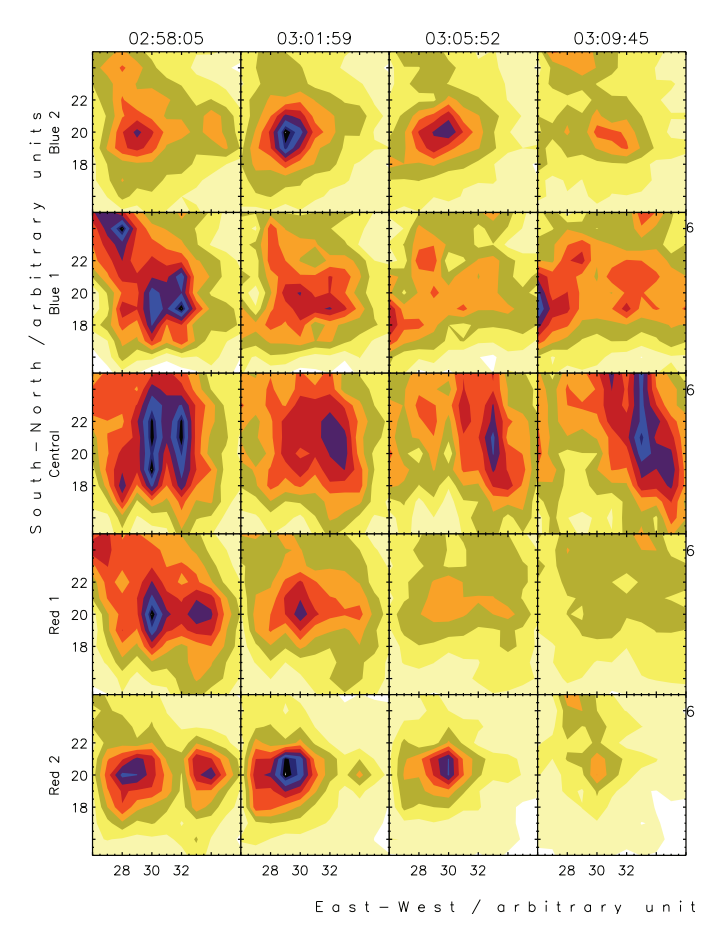


Figure 1. Two dimensional distributions for an EE observed on 26 June with 40 EW positions. Each column corresponds to a different time interval (given at the top) and each row to a given spectral channel, indicated at the left. Blue 1 and Red 1, in this figure, correspond to 45 km s⁻¹, blue and red Doppler shifts, respectively, and Blue 2 and Red 2 to 72 km s⁻¹.

may be seen that at the end of this EE (right panels) the rest velocity emission at the West side remains high.

It is observed, at some EE, that the growing phase of the rest velocity amplitude lasts more than blue and red ones. In the left panel of Figure 3 the maximum amplitudes for the 45 km s⁻¹ blue distributions, before, during and after the maximum of an EE, are shown. The maximum amplitudes at the same time intervals, for the rest Doppler velocity (middle panel) and for the 45 km s⁻¹ red distributions (*right panel*), are shown. The time is given at the x-axis in arbitrary units, at the y-axis the amplitudes, also in arbitrary units, are given. It may be seen, from this figure, that blue and red amplitudes reach a maximum value and then decrease. On the other hand, the amplitude of the rest Doppler velocity keeps growing while blue and red are decreasing.

In the *left panel* of Figure 4 the NS blue distributions at $\sim 2''$ from the maximum and one minute after it are shown. In the *middle panel* the NS distributions for a location near an EE are shown, an offset of the source maximum is also seen. The source width

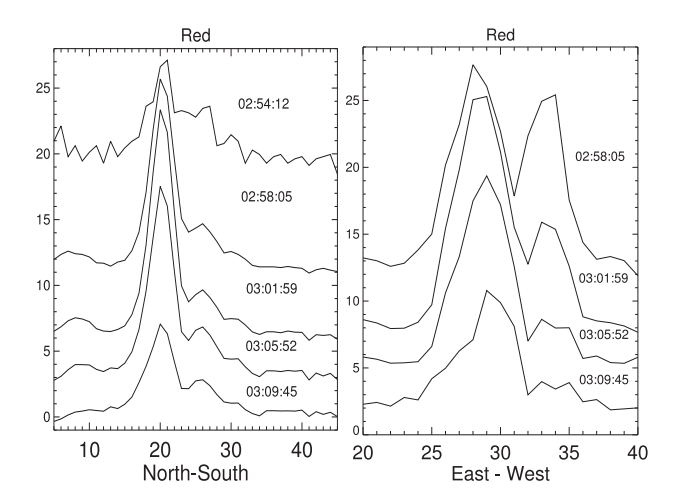


Figure 2. *Left panel*: NS distributions for the red wavelength at the EE of Figure 1. *Right panel*: EW distributions for the same EE, at the same wavelength. In this and in the next figures the x-axis scale is given in arcseconds while in the y-axis the amplitudes, in arbitrary units, are given. Times are given at each distribution. It may be seen that at the middle distribution of the *left panel*, the amplitude is higher than before and after it.

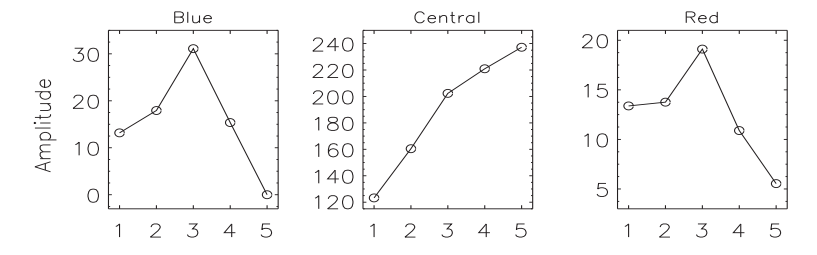


Figure 3. *Left panel*: Maximum amplitudes for the 45 km s⁻¹ blue distributions, before, during and after the maximum of an EE. *Middle panel*: Maximum amplitudes for the rest Doppler velocity distributions. *Right panel*: Maximum amplitudes for the 45 km s⁻¹ red distributions of the same EE.

increases as the velocity decreases. On the right panel, NS distributions are shown. Contrary to the previous distributions, in this case the amplitudes for the 0 to $18~\rm km~s^{-1}$ sources are similar to each other.

In Figure 5 the one-dimensional NS distributions after the maximum of an EE are shown. The amplitudes correspond to the 0-36 km s⁻¹ blue (*solid*) and red (*dashed*) channels. There is an offset between blue and red sources which increases with velocity, the offset reaches the maximum at ~ 40 km s⁻¹ following a linear relation. The same behavior is seen at other EE.

In Figure 6 the red distributions for times before and after an EE are shown. Two sources are seen, the Southern one is more intense prior the EE maximum and decreases with time, while the Northern source increases and becomes more intense that the Southern after the maximum. Distributions that indicate the presence of two sources are seen at other EE. At Figure 7 a cartoon of a possible situation for the appearance of two sources is shown.

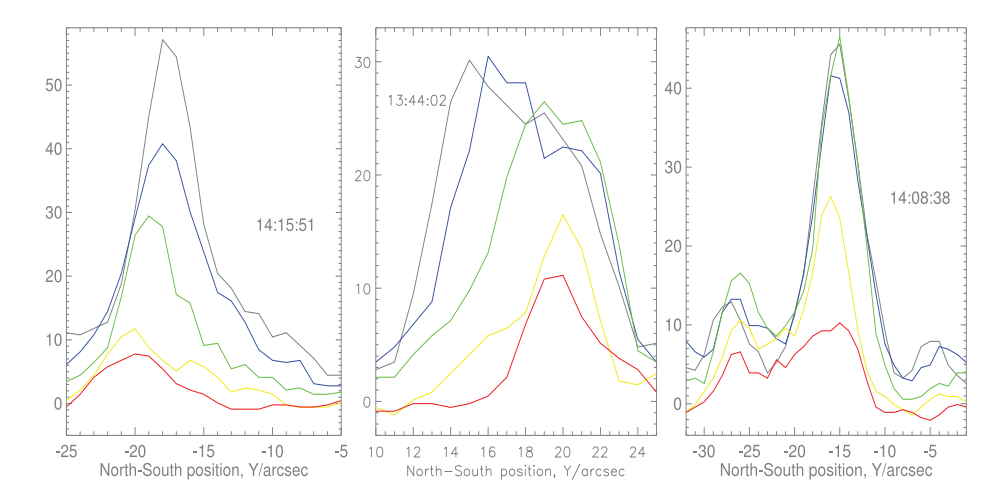


Figure 4. Left panel: NS blue (continuous lines) and red distributions (dashed lines) observed $\sim 0.8"$ on the East of an EE maximum, 1.6 minutes after it. It may be seen that the blue distributions are at the South respect the red ones. Middle panel: NS red distributions observed about two minutes after an EE maximum. The maxima are offset respect each other. Right panel: NS red distributions seen one minute after an EE maximum at $\sim 1"$ from it. In this case the amplitudes for the 0-18 km s⁻¹ range are similar.

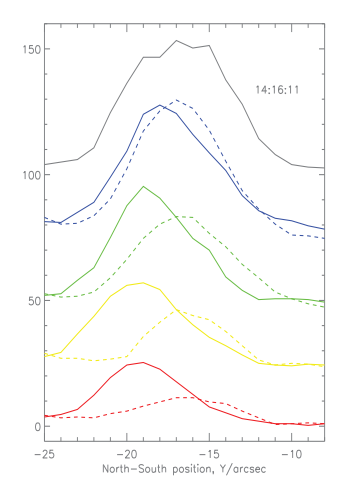


Figure 5. NS blue (*solid lines*) and NS red distributions (*dashed lines*) observed $\sim 0.8''$ on the East of an EE maximum, 1.6 minutes after it. *Black lines* are for the rest Doppler velocity, blue for 9 km s⁻¹, green for 18 km s⁻¹, yellow for 27 km s⁻¹ and red for 36 km s⁻¹. It may be seen that the blue distributions are at the South respect the red ones. The offset between red and blue maxima is larger for the high velocity sources.

From Figure 1 it may be seen that the central wavelength source is larger than blue and red sources. This situation is seen at most of the EE sources at the different stages and it was earlier observed. The Full Width at Half Maximum (FWHM), of the sources at the EE maximum, was measured across NS and EW directions to estimate the source sizes. The widths for the time of the maximum are shown in Figure 8. It

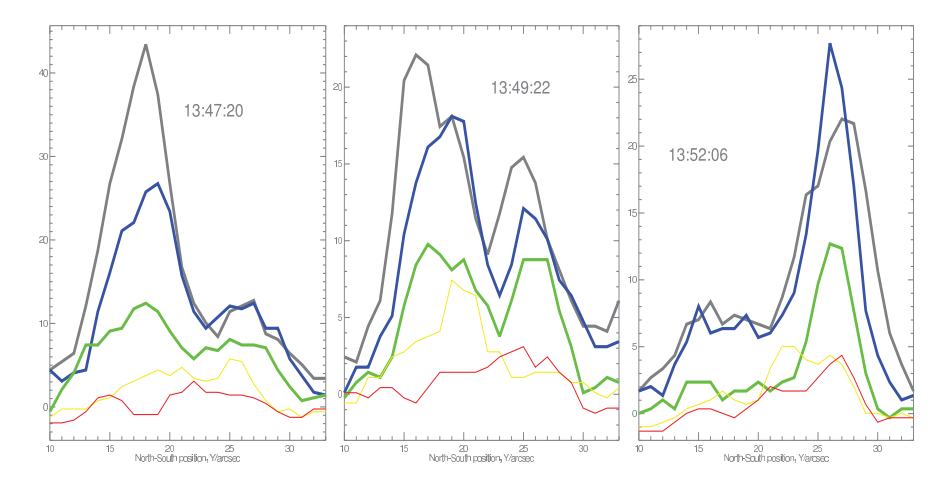


Figure 6. Red distributions observed $\sim 1.5''$ from an EE maximum, 0.8 min before (*left*), 1.3 min after (*middle*) and 4 minutes after the time of the EE maximum (*right*).

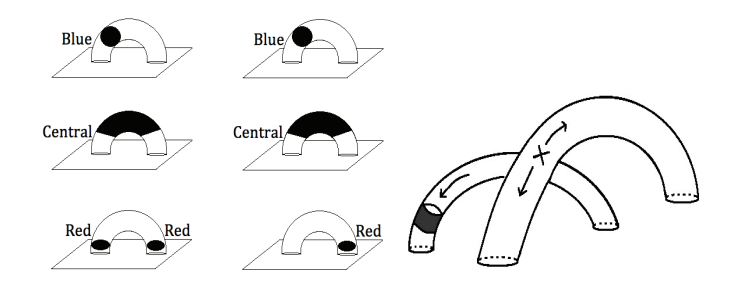


Figure 7. *Left panel*: A sketch of the possible scenario for the first and second frames of the EE of Figures 1 and 2. *Right panel*: Two interacting loops where an EE is taking place. Such situation could lead to the occurrence of similar amplitudes for different velocity sources at about 1" from the maximum, as seen in the *right panel* of Figure 4. The shadow at the small arc denotes the region where the amplitudes of the 0-18 km s⁻¹ sources are similar to each other.

may be seen that, for blue sources, the NS sizes are larger than EW ones. A similar situation, but not as clear, is seen for red sources. This could be due to the geometry of the sources. However, up to now we can not rule out the possibility that the regime of the observations could also play a role.

In Figure 9 the field of view scanned on June 27 at the North-West of the solar disk is shown. The limb is at the right-upper corner, so that the white region at this corner is outside the solar disk. Various EE are seen at this field. At the NS distributions the sources are well outlined (similar to the source at the *left panel* of Figure 2). However, in EW direction the sources are seen near to other varying local maxima. This could happen if sources, as those at the bottom panels of Figure 1, would be at the legs of arcs that are predominantly EW oriented. Then, as the arc is close to the West limb, for the observer the sources at the legs would become closer and closer with respect to each other.

It may be seen from Figure 9 that, at all the wavelengths drawn, the sources are elongated parallel to the limb. The blue emission is more extended than the red one.

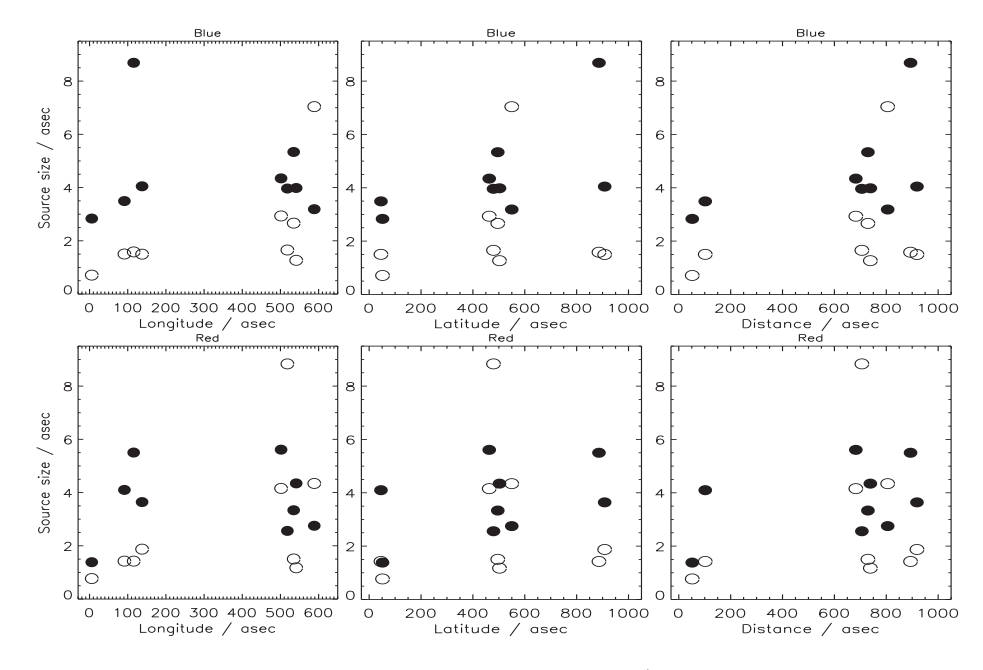


Figure 8. *Upper panels*: The sizes of the 63 km s⁻¹ blue sources at maximum radiance as a function of longitude (*left*), latitude (*middle*) and distance to the disk center (*right*). Filled circles are for NS and empty for EW widths. *Lower panels*: The sizes of the 63 km s⁻¹ red sources as a function of longitude (*left*), latitude (*middle*) and distance to the disk center (*right*).

However, the sources at the South of the field (at NS locations between 50 and 60) are more clearly seen at red than at blue wavelengths. For the field near this limb the above situation is common, i.e., the EE red sources are more compact than blue ones but more clearly seen.

The central distributions show some features like filaments that resemble spicules. The Red 1 distributions (45 km s^{-1} in this case) are more similar to the central wavelength distributions than the blue ones. The same is seen at other EE sources. This result could indicate that the emission at the rest Doppler velocity is more similar, and possibly dependent, to the low velocity red sources than to the blue ones.

4. Discussion

Some characteristics of the sources are commonly observed at EE. Offsets of different velocity sources may be seen before (up to ~ 5 minutes), during and after (up to ~ 5 minutes) the maximum at locations from the maximum itself to about 2" from it. After the EE maximum, at some locations around it, the distributions show two sources. This situation may be explained as a result of sources at different legs of a magnetic arc. A cartoon to explain this, for the particular case of the EE of Figure 1, is given at the left side of Figure 7. Also, at various EE, similar shapes and amplitudes at distributions with 0-18 km s⁻¹ are seen after the maximum (up to ~ 3 minutes) at about 1" from it. A possible interpretation of this result is given at the right side of Figure 7.

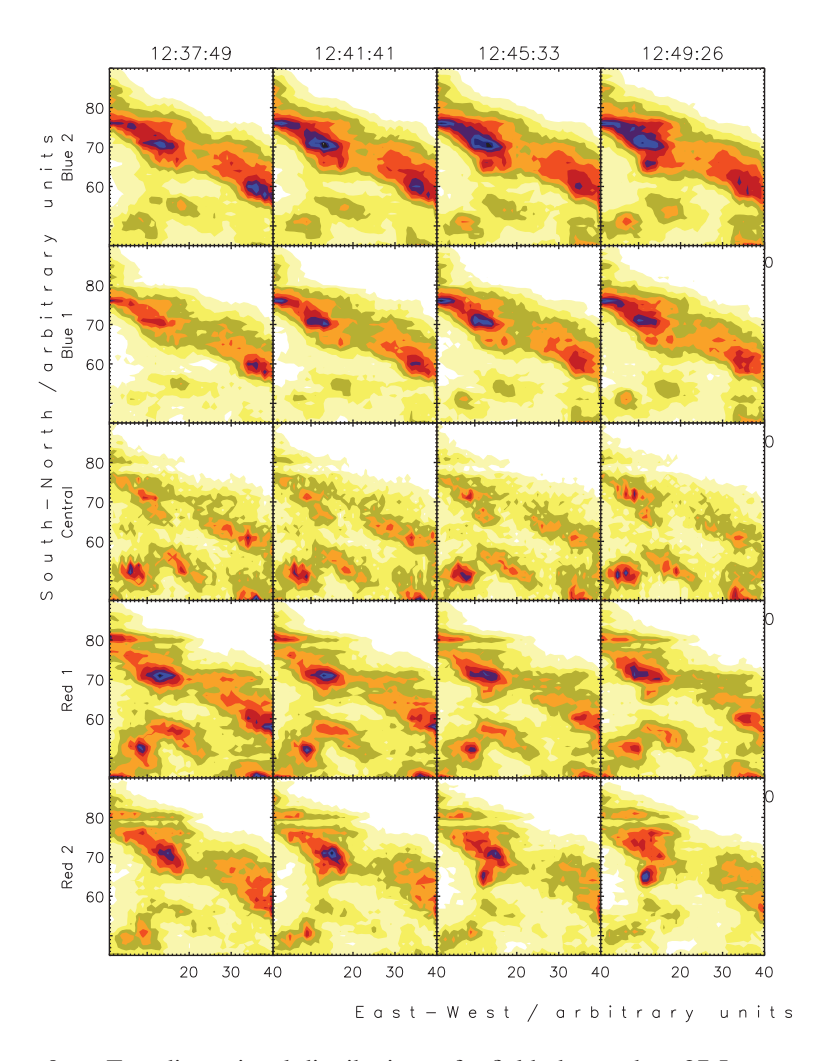


Figure 9. Two dimensional distributions of a field observed on 27 June near the limb. The white region is outside of the solar disk.

A source inside an arc could be the origin of the relation between the offsets and velocities as follows. For example, for a source moving inside an arc with constant lineal velocity (v_0), the projected velocity would depend on the angle between the arc and the observer.

If the observer sees to the apex of a circumference, the Doppler velocity (v_r) and the projected distance to the center (r) would be related by $v_r = v_0 \frac{r}{r_0}$, where r_0 is the loop radius. From the one-dimensional distributions (for example, the distributions on the left panel of Figure 4) we found a linear relation between the source offsets and their velocities which follows well the above relation for a source inside an arc.

The cases where sources with similar $0-18 \text{ km s}^{-1}$ distributions are seen, could be the result of a slowing down flow. An scenario of two interacting loops where one is small could lead to the conditions for this (Figure 7). At low altitudes, the high density would slow down the flow that is going to lower layers in the small magnetic loop,

leading to a rapid decrease of the velocity. In the right panel of Figure 7 the region of the brake down is depicted as a shadow in the small arc.

References

Chae, J., Wang, H., Lee, C.-Y., Goode, P. R., & Schuehle, U. 1998a, ApJ, 497, L109 Chae, J., Wang, H., Lee, C.-Y., Goode, P. R., & Schuhle, U. 1998b, ApJ, 504, L123 Innes, D. E., Brekke, P., Germerott, D., & Wilhelm, K. 1997, Solar Phys., 175, 341 Mendoza-Torres, J. E., Torres-Papaqui, J. P., & Wilhelm, K. 2005, A&A, 431, 339 Porter, J. G., & Dere, K. P. 1991, ApJ, 370, 775